



## Coastal flooding: impact of waves on storm surge during extremes. A case study for the German Bight

5 **Joanna Staneva<sup>1</sup>, Kathrin Wahle<sup>1</sup>, Wolfgang Koch<sup>1</sup>, Arno Behrens<sup>1</sup>, Luciana Fenoglio-Marc<sup>2</sup> and Emil V. Stanev<sup>1</sup>**

1. Institute for Coastal Research, HZG, Max-Planck-Strasse 1, D-21502 Geesthacht, Germany

2. Institute of Geodesy and Geoinformation, University of Bonn, Nussallee 17, D- 53115 Bonn, Germany

Correspondence to: J. Staneva (joanna.Staneva@hzg.de)

10

### Abstract

This study addresses impact of wind, waves, tidal forcing and baroclinicity on the sea level of the German Bight during extremes. The role of waves-induced processes, tides and baroclinicity is quantified and the results are compared with observational data that include various in-situ  
15 measurements as well as satellite data. A coupled, high-resolution, model system is used to simulate the wind waves, water level and three-dimensional hydrodynamics. The effects of the wind waves on sea level variability are studied accounting for wave-dependent stress, wave-breaking parameterization and wave-induced effects on vertical mixing. The analyses of the coupled model results reveal a closer match with observations than for the stand-alone  
20 circulation model, especially during the extreme storm Xaver in December 2013. The predicted surge of the coupled model enhances significantly during extremes when considering wave-current interaction processes. The wave-dependent approach yields to a contribution of more than 30% in some coastal area during extremes. The improved skill resulting from the new developments justifies further use of coupled wave and three dimensional circulation models for  
25 improvement of coastal flooding predictions.



## 1. Introduction

A challenging topic in coastal flooding research is the provision of accurate predictions of the sea surface elevations and wave heights. This is highly relevant over the European shelf that is characterized by vast near-coastal shallow areas and large near coastal urban population. The increased demand of improving wave and storm predictions requires further development and improved representation of the physical processes in the ocean models. The wind-induced surface stress plays an important role at shallow area (e.g. Flather, 2001). The importance of wind wave-induced turbulence for the sea surface has been demonstrated by Davies et al. (2000); for the bottom layer by Jones and Davies, (1998); and for the wave-induced mixing by Babanin, (2006) and Huang et al. (2011). Qiao et al. (2004) developed a parameterization of wave-induced mixing from the Reynolds stress induced by the wave orbital motion, and coupled this mixing to circulation model. They found that the wave-induced mixing can greatly enhance the vertical mixing in the upper ocean.

Understanding waves-current interaction processes is important for coupling between the different earth system components (e.g. ocean, atmosphere, wave models) and further integrating of biogeochemical or morphological parts. Longuett-Higgins and Stewart (1964) showed that wave dissipation induced gradients of radiation stress that accounts for a transfer of wave momentum to the water column, changing the mean water level. The effects of waves on the wind boundary layer are demonstrated by number of studies like Janssen 2004, Donelan et al., 2012; Fan et al., 2009. The effects of wave-current interactions caused by radiation stresses have been also addressed by Brown and Wolf, 2009, Wolf and Prandle, 1999. A vortex force formulation was used by Bennis and Arduin (2011); McWilliams et al., 2004; Benetazzo et al. 2013). The comparisons of both methods by Moghimi et al. (2013) showed that for the longshore circulations the results are similar, however enhanced offshore directed transport in the wave shoaling regions is simulated using radiation stress approach.

Many other studies based on theoretical and practical analyses dealt with the role of interaction between wind waves and circulation for the ocean state (Michaud et al., 2012, Barbariol et al. 2013; Brown et al, 2011; Benetazzo et al. 2013; Katsafados et al., 2016; Bolaños et al., 2011, 2014). The role of wave-induced processes on Lagrangian transport and particle distributions is demonstrated by Röhrs et al. (2012, 2014). For idealized conditions, Weber et al, (2008)



performed Lagrangian analysis of the mean drift due to dissipating surface gravity waves and showed that mean Lagrangian wave setup of the free surface and the mean drift solutions in a rotating ocean are given for a steady balanced flow; later Weber et al (2015) demonstrated by comparison with Lagrangian results that Coriolis Stokes force acts to change the vertically-integrated Eulerian kinetic energy of the mean flow. The importance of waves-current interaction of turbulence and bottom stress is shown by Babanin et al. (2010).

It is well accepted that a storm surge is meteorologically driven – typically by wind and the atmospheric pressure. With further development of coastal economic and concentration of population in the coastal areas, dikes were built to protect from flooding. Even since, keeping dikes in order was a challenge, and keeping the dangers of storm surges at bay became an important issue (Storch, 2014). IPCC (2014) summarized that on regional scales it was very likely that there would be an increase in the occurrence of future sea level extremes in coastal regions by 2100 though and demonstrated the low confidence in region-specific projections in storminess and storm surges, thus more and more seawalls and levees would be overtopped in 2100 (Wang et al., 2012). Moreover, wave and tides would be amplified by the rise in sea level, which could increase the rate and intensity of this process, causing the collapse and damaging the seawalls/levees. Improved wave and circulation forecasts for the North Sea and its coastal areas, especially within the German Bight are of greatest importance for marine and coastal environment and can reduce the damages caused by flooding or coastal erosions. This is of utmost importance for example for the off-shore wind energy, ship navigations, and coastal zone protections. Surge and tidal combinations is known as “still water level” since in contrast to the very short wave period of 1-20 s, the periods of the water level vary from several hours to days. Further superimposed by waves can additionally contribute to water level increase, causing further coastal flooding. Waves combined with higher water levels may break dykes, causing flooding and damaging and destroying constructions, coastal erosions (Pullen et al, 2007). The wave impact includes also wave breaking and changes of the beaches, increasing the coastal erosion and modifying the sediment dynamic (Grashorn et al., 2015; Lettman et al., 2009).

The German Bight area is dominated by strong north-westerly winds and external waves due to the Northeast Atlantic low pressure systems (Rossiter, 1958; Fenoglio-Marc et al., 2015). Extratropical cyclones in the area are substantial hazard especially for the shallow coastal Wadden Sea areas (Jensen and Mueller-Navarra, 2008). The coastal flooding can be caused by the combined



5 role of wind waves together with high tides and storm surges in response to fluctuations in local  
and remote winds and atmospheric pressure cause. The role of those processes can be assessed  
by using high resolution coupled model coastal systems. However, in the frame of forecasting  
and climate modelling studies, the different processes of wave and current interactions are still  
not sufficiently exploited. In this study, we address the wave-current interaction processes in  
order to assess their impact on the sea level of the German Bight during extremes. We quantify  
their individual and collective role and compare the model results with observational data that  
include various in-situ measurements as well as satellite data. The wave model (WAM) and the  
circulation model (GETM), the processes of their interaction, the study period as well as the  
10 different model experiments are presented in Section 2. The observational data that have been  
used are described in Section 3, followed by model-data comparisons in Section 4. Finally  
Section 5 addresses the effects of the different physical processes on the sea level variability;  
followed by concluding remarks.

## 15 2. Models

### 2.1 Hydrodynamical Model

The circulation model used in this study is the General Estuarine Transport Model (GETM,  
Burchard and Bolding, 2002). The German Bight model set-up has a horizontal resolution of 1  
km and 21  $\sigma$ -layers. GETM uses the  $k$ - $\epsilon$  turbulence closure to solve for the turbulent kinetic  
20 energy  $k$  and its dissipation rate  $\epsilon$ . The open boundary data for temperature, salinity, velocity and  
sea surface elevation are obtained from the coarser resolution (ca 5 km and 21  $\sigma$ -layers) North  
Sea-Baltic Sea outer model. Those models are described in details by Staneva et al. (2009); see  
also Fig. 1 for the bathymetry map of the German Bight model domain. Both models were forced  
by are-sea interaction fluxes that are estimated using bulk aerodynamic formulas. The  
25 atmospheric data needed to estimate those fluxes are taken from the German Weather Service  
(DWD; Deutscher Wetter Dienst) and have a horizontal resolution of 7 km. The river run-off  
data were provided by the German Maritime and Hydrographic Agency (BSH, see also Staneva  
et al., 2016)



## 2.2 Wave Model

Ocean surface waves are described with the two-dimensional wave action density spectrum  $N(\sigma, \theta, \varphi, \lambda, t)$  as a function of relative angular frequency  $\sigma$ , wave direction  $\theta$ , latitude  $\varphi$ , longitude  $\lambda$  and time  $t$ . The appropriate tool to solve that balance equation is the well-established advanced third generation spectral wave model WAM (WAMDI group, 1988, ECMWF, 2015). The use of the wave action density spectrum  $N$  is required if currents have to be taken into account. In that case the action density is conserved in contrast to the energy density which is normally used in the absence of time-dependent water depths and currents. The action density spectrum is defined as the energy density spectrum  $E(\sigma, \theta, \varphi, \lambda, t)$  divided by  $\sigma$  observed in a frame moving with the ocean current velocity (Whitham, 1974, Komen *et al.*, 1994) :

$$N(\sigma, \theta) = \frac{E(\sigma, \theta)}{\sigma} \quad (1)$$

The wave action balance equation in Cartesian coordinates is given as:

$$\frac{\partial N}{\partial t} + (\mathbf{c}_g + \mathbf{U}) \nabla_{x,y} N + \frac{\partial c_\sigma N}{\partial \sigma} + \frac{\partial c_\theta N}{\partial \theta} = \frac{S_{wind} + S_{nl4} + S_{wc} + S_{bot} + S_{br}}{\sigma} \quad (2)$$

The first term on the left-hand side of equation (2) represents the local rate of change of action density; the second one describes the propagation of wave energy in the two dimensional geographical space, where  $\mathbf{c}_g$  is the group velocity vector and  $\mathbf{U}$  the corresponding current vector. The third term of the balance equation denotes shifting of the relative frequency due to possible variations in depths and currents (with propagation velocity  $c_\sigma$  in  $\sigma$  space). And the last term on the left-hand side of the equation finally represents depth induced and current-induced refraction (with the propagation velocity  $c_\theta$  in  $\theta$  space). The term  $S = S(\sigma, \theta, \varphi, \lambda, t)$  on the right-hand side of (2) is the net source term expressed in terms of action density. It is the sum of a number of source terms representing the effects of wave generation by wind ( $S_{wind}$ ) quadruplet nonlinear wave-wave interactions ( $S_{nl4}$ ), dissipation due to white capping ( $S_{wc}$ ), bottom friction ( $S_{bot}$ ) and wave breaking ( $S_{br}$ ). The current version of the third generation wave model WAM Cycle 4.5.4 is an update of the former Cycle 4 that is described in detail in Komen *et al.* (1994) and Guenther *et al.* (1992). The basic physics and numerics are kept in that new release. The source function integration scheme is provided by Hersbach and Janssen (1999), and the up-dated source terms of Bidlot *et al.* (2007) are incorporated. The wave model has the same resolution, utilizes the same



bathymetry and wind forcing as the GETM model. The boundary values of the North Sea model are taken from the operational regional wave model of the DWD.

### 2.3 Coupled wave-circulation model implementation

5 The implementation of the depth dependent equations of the mean currents  $\mathbf{u}(\mathbf{x}, \mathbf{z}, \mathbf{t})$  in the presence of waves follows Mellor (2011). Starting with the momentum equation for an incompressible fluid  $d\mathbf{u}/dt = \mathbf{F} - \nabla\delta p$ , where  $\mathbf{F}$  states for the sum of external forces (Coriolis, gravity, friction) and  $\nabla\delta p$  is the pressure gradient, which includes the influence of the wave motion on the mean current. Using linear wave theory and accounting for second order terms of wave height the equation of motions then reads

$$\frac{\partial\langle\mathbf{u}\rangle}{\partial t} = \langle\mathbf{F}\rangle - \langle\mathbf{u}\rangle \cdot \frac{\partial\langle\mathbf{u}\rangle}{\partial\mathbf{x}} - \frac{\partial}{\partial\mathbf{x}} \cdot \mathbf{S}, \quad (3)$$

10 where the angle brackets denote averaging over the wave period, thus  $\langle\mathbf{u}\rangle$  is the sum of the Eulerian current and the Stokes drift  $2\omega k H_s^2 / (\sinh^2 kD)$  for waves with angular frequency  $\omega$ , wavenumber  $k$  and significant wave height  $H_s$  in a water column of depth  $D$ .  $\mathbf{S}$  is the radiation stress tensor:

$$\mathbf{S} = E \left( \frac{c_f}{c_g} \left[ \frac{\mathbf{k} \otimes \mathbf{k}}{k^2} + \delta \right] \frac{\sinh 2kh + 2kh}{\sinh 2kD + 2kD} - \delta \frac{\cosh 2kh - 1}{4 \sinh^2 kD} \right), \quad (4)$$

15 with  $E = 1/16gH_s$  the wave energy, wave vector  $\mathbf{k}$  and  $h = D(1 + \xi)$  is the local depth of layer  $\xi$ . Thus the divergence of the radiation stress is the only (to second order) force related to waves in the momentum equations. The equation for kinetic energy, which is derived from the momentum equation by multiplication with the velocity vector, reads

$$\frac{\partial E_{kin}}{\partial t} = \langle\mathbf{F}\rangle \cdot \langle\mathbf{u}\rangle - \langle\mathbf{u}\rangle \cdot \frac{\partial E_{kin}}{\partial\mathbf{x}} - \frac{\partial}{\partial\mathbf{x}} \cdot \mathbf{S} \cdot \langle\mathbf{u}\rangle, \quad (5)$$

20 where gradients in wave energy (*i.e.* dissipation due to wave breaking) may lead to increased surface elevations (wave setup).

The necessary wave state information to account for the divergence of the radiation stress in the GETM momentum equations is provided by WAM. WAM gives also data



on dissipation source functions (wave breaking and white capping as well as bottom  
dissipation) to the turbulence module GOTM. There it is used for the calculation of  
boundary conditions for the dissipation of turbulent kinetic energy and the vorticity due  
to wave breaking and due to bottom friction (Pleskachevsky et al., 2011).  
5 Additionally, bottom friction depending on bottom roughness and wave properties)  
have been implemented (Styles and Glenn, 2000).

#### 2.4 Study period (meteorological conditions)

This study is focused on the period during the winter storm Xaver on the 5th and 6th of  
10 December, 2013, causing flooding and serious damages in the southern North Sea coastal areas.  
During 4th to 7<sup>th</sup> of December, the storm depression Xaver moved from the south of Iceland over  
the Faeroe Island to Norway and southern Sweden and further over the Baltic Sea to Estonia,  
Latvia and Lithuania. It had its lowest sea level pressure on 5 December 18 UTC over Norway  
(ca. 970 hPa, Figure 2 and 3). It is interesting to notice here that over the German Bight area the  
15 storm Xaver coincided with high tides and thus an extreme weather warning was given to coastal  
areas of north western Germany due to more than 130 km/h recorded wind gusts (Deutschländer  
et al., 2013). The extremely high water level and waves triggered sand-displacements on the  
barrier islands and erosion of dunes in the Wadden Sea regions. The German Weather Service  
reported the storm to be worse or similar to what has been experienced during the North Sea  
20 flood of 1962 in which 340 people lost their lives in Hamburg, saying that improvements in sea  
defences since that time would withstand this storm surge (Deutschländer et al., 2013, Lamb and  
Frydendahl, 1991).

#### 2.5 Numerical experiments

25 For the control simulation (CTRL run), GETM is run as fully three dimensional baroclinic model  
without a wave model as described in Section 2.1. The fully two-way coupled GETM-WAM  
model simulations account for the processes as described in Section 2.3. The coupling is  
performed via the coupler OASIS3-MCT: Ocean, Atmosphere, Sea, Ice, and Soil model at the  
European Centre for Research and Advanced Training in Scientific Computation Software,  
30 (Valcke et al., 2013).



5 The effects on using different coupling methods are studied by comparing the two-way fully coupled GETM-WAM model simulations (FULL run) with the one-way coupled model, in which the circulation model obtains information from the wave model WAM (one-way coupling); we name this experiment further as FORCED run. Additionally we run the circulation model GETM as a two-dimensional barotropic model (so called 2D run). In the last experiments we excluded the river run-off forcing (NORIV run). The list of these experiments is given on Table 1.

### 3. Observational data

10 The tide gauge observations from the eSurge project ([www.esurge.org](http://www.esurge.org)) are used. An overview of existing operational tide gauges in the North Sea and Baltic Sea regions available at the webpages of the EuroGOOS regions NOOS (North West Shelf Operational Oceanographic System) and BOOS (Baltic Operational Oceanographic System), respectively: [www.noos.cc](http://www.noos.cc) and [www.boos.org](http://www.boos.org). The water level data used here were acquired through the NOOS ftp server.

15 The in-situ wave data are taken from the wave-buoy observational network operated in the North and Baltic Seas by the BSH: (<http://www.bsh.de/de/Meeresdaten/Beobachtungen>).

Additionally for validation we used satellite measurements of significant wave height and sea level in the German Bight area derived from the Jason-2, CryoSa-2 and SARAL/AltiKa altimetry satellite missions, . This last is here of special interest since the satellite passed over the North  
20 Sea at the time of storm Xaver. As in Fenoglio-Marc et al. (2015), the standard altimeter products were extracted from the Radar Altimeter Database System (RADS) (Scharroo, 2013). The sea water level corresponding to the instantaneous in-situ tide gauge measurement, and called Total Water Level Envelope (TWLE) in Fenoglio-Marc et al. (2015), has been estimated as the difference between orbital altitude above the mean sea surface model DTU10 and the radar  
25 range corrected for ionospheric and tropospheric path delay, solid Earth, sea state bias and load tide effects. Corrections for ocean tide and for atmospheric inverse barometer effect and wind have not been applied. Further on, the storm surge has been estimated correcting the TWLE for the ocean tide given by the global ocean tide model GOT4.8 (Ray et al., 2011), see Fenoglio-Marc et al (2015) for more details.

30



## 4. Model validation during the extreme

### 4.1 Wave model performance

In this section, we will analyse the wave model performance during Xaver. The significant wave heights ( $H_s$ ) from the model simulations are in good agreement with the measured values. As an example we present time-series graph for stations Elbe (top) and Westerland (bottom) during 2-8 December, 2013 (Fig. 4). During the extreme, the measured  $H_s$ , was above 7.5 m. It is noteworthy that the wave model over-predicts the storm peak  $H_s$  (Fig. 4 b,d), due to the DWD winds which are over-estimated in storm conditions (Staneva et al., 2016). In addition, the maximum of the statistical wave height simulated by the model for the two locations (Fig. 4a,c) occurs earlier than the one of the measurements, which is due to shifted maximum of the DWD wind forecasts. The standard deviation between the model and the measurements is 0.16 m for the Elbe and 0.12 m for the Westerland station. The correlation coefficients between the WAM simulations and measurements were always high - above 0.9 for all stations and the normalized RMS error was relatively low. For analyses on the wave model performance including different statistical parameters computed during the extreme event for all available German Bight stations we refer to Staneva et al. (2016).

The wave spectra at the locations of FINO-1 and Elbe BSH buoy stations are given in Fig. 5 for the study period. The wave spectra from the model simulations (Fig.5a, c) are in a good agreement with the spectra from the observations (Fig.5a, c). The time variability of spectral energy is well reproduced by the model and the energy around the peak is similar in observations and simulations; however the model patterns are smoother than the observed ones.

In addition to the in-situ measurements, the satellite altimetric data provide a unique opportunity to evaluate both temporal and spatial variability simulated in the model along its ground-track at the time of the overflight of the German Bight lasting around 38 sec (see Figure 6 a, b). The modelled significant wave height ( $H_s$ ) varies along the satellite ground-tracks between 1.2 and 1.9 m during calm conditions on 03. December 2013 at 18:00 UTC (Fig. 6a), while for the period of extreme storm Xaver  $H_s$  varies between 6.3 m and 9.4 m (06. December 2013 at 04:00 UTC, Fig. 6b). The spatial distribution of the wave model results (Fig.6c, d) is in good agreement with the satellite data in both cases. The latitudinal distribution of  $H_s$  by the model (green dots) is smoother than the one of the satellite data, which can be explained by the different way of post-processing of the satellite data of significant wave height and by the statistical nature



of its estimate by the model. For calm conditions (Fig.6 c)  $H_s$  is slightly underestimated (ca. 15 cm) in the coastal area and overestimated (ca. 20 cm) in the open German Bight. During Xaver the model slightly overestimates the satellite data in the open areas (with ca. 20-30 cm). These results are in good consistency with results shown in Fenoglio-Marc et al. (2015) who compared the SARAL data with the DWD wave simulations.

#### 4.2 Sea level and wave induced forcing

In this section, we will demonstrate the performance of the hydrodynamic model to simulate the mean sea level and give statistics obtained for the whole integration period. Detailed statistical analyses on model comparisons with measurements are quantified by Staneva et al. (2016), where the performance of the wave and hydrodynamical model results for the area of German Bight is shown to be in a good agreement with observations not only during the calm conditions, but most importantly, during storm events. Therefore here we will only provide new examples on model-data validations, including also satellite data that have not been used in the previous studies.

The geographical representation of the bias between the model simulations and all available tide gauges data shows that the bias for most of the tide gauge stations is within the range of  $\pm 0.1$  m, (Fig. 7). Exceptions are found in some coastal tide gauge data stations in the very shallow areas. This can be attributed to the relatively coarse spatial resolution (1 km) and consequently smoother model bathymetry in the shallow coastal waters. From the simulations and tide-gauge observations, storm surges were estimated by subtracting the ocean tide estimated using the T\_TIDE routine (Pawlowicz et al., 2002). From the surge model comparisons with the satellite data shown on Figure 8, it can be concluded that the model results are in a very good agreement with the observations both during calm conditions (at 03.12.2013), where the surge has relative small values (less than 10 cm offshore and up to 25 cm near the coastal area, Fig. 8c) and most importantly, during the storm Xaver at 06.12.2013, where the surge reached almost 3 m. Statistics from the comparisons between observations and the different experiments are presented on Tables 2. The results demonstrate that the coupling between circulation and waves improves significantly the surge predictions; once the effects of interaction with waves are considered both the BIAS and the RMSE are reduced.



5 The time evolution of the water level for the Helgoland tide gauge data (see Fig. 1 for its location) is shown in Fig. 9. The consistency between the model simulations from both CTRL and FULL runs is very good during normal meteorological conditions. During the storm event however, the water level simulated by the stand-alone circulation model is lower by about 30 cm compared to the data from the Helgoland tidal gauge station. Once the wave-induced processes are taken into consideration, the simulated sea level (FULL run) is closer to the observations. Including wave-current interaction processes improved the root mean square errors and the correlation coefficient between the tide gauges data and the simulated sea level over the German Bight area (Table 2).

10 The surge height reaches values of about 2.5 m during Xaver and has its maximum at low water. It is noteworthy that during the Xaver event two maxima of the surge ( $S_{\max 1}$  and  $S_{\max 2}$  in green line Fig. 9) have been observed. Fenoglio et al. (2015) described the first surge maximum as a wind-induced one. They noticed also that, instead, at the Aberdeen and Lowestoft, stations, the surge derived from the tide-gauge records had only one maximum, It reached reaching the

15 eastern North Sea coastal areas (anticlockwise propagation) about ten hours later than in Lowestoft (easternmost UK coast) and finally, causing the second storm surge maximum that has been detected by the measurements in the German Bight area. As shown in Staneva et al. (2016) the wave-induced mechanisms contribute to a persistent increase of the surge after the occurrence of the first maximum (with slight overestimation after the second peak). At the two

20 maxima the observed water level at the Helgoland tide gauge is in better agreement with the coupled model (FULL run- the black line) than with the CTRL simulated water level. The two maxima are underestimated by the stand-alone circulation model (CTRL-red line) especially at high water, where the surge difference between the model results and the measurements is about 30 cm for the first peak and more than 40 cm during the second peak (Fig. 9).

25

## 5. Process studies

### 5.1 Sensitivity of surge predictions to coupling with waves

30 In this section we will analyse the role of wave-current interaction in the storm surge model and will also demonstrate their sensitivity to one-way versus two-way coupling. Fig. 10 shows time series of water height (black line) and the storm surge (red line) for six stations (see Fig. 1 for their locations) together with the differences of the surge between the FULL and CTRL runs



(FULL-CTRL, green line) and the differences between the FULL and FORCED runs (FULL-FORCED, blue line). The surge during the extreme exceeds 2 m in the open-ocean stations and increases with up to 2.8 m in the proximity of the coastal stations. The two separate storm surge maxima during the Xaver storm (as described in Section 4) are clearly seen in the near coastal stations ST1-4, whereas for ST6 (in the Elbe Estuary), the surge is kept at high values even in the period between the two maxima. The coupling with waves approach leads to a persistent increase of the surge especially after the occurrence of the first maximum (Smax1). The difference in surge between the FULL and CTRL runs (green line) reaches maximum during the first peak of the surge and is substantial during the follow-up two days. For the Hörnum station (ST3) the raise of the surge due to coupling with waves exceeds 35% compared to CTRL data (Fig. 10c), At the north-easternmost station (ST4), the surge difference between FULL and CTRL runs is more than 70 cm which gives a contribution of the wave-current interaction processes of more than 40%. For the open deeper water station (ST5, Fig. 10f), the maximum contribution is about 30 cm- that makes 25% increase of the surge. The differences between FORCED and FULL runs are relatively small (less than 4% of the total for all stations-see the blue line). However, for the shallower Elbe Station (ST6, Fig. 10e) the effects of two-way coupling in comparissons to the FORCED run (one-way coupling) seem important.

To give an illustration of the coastal impact caused by the storm Xaver, we analyse the horizontal patterns of maximum storm surge (Fig. 11) over the four tidal periods T1-T4 (as specified in Fig 9). During the second peak (T3), the surge exceeds 2.8 m over the whole German Bight coast (Fig. 11c), the storm surge for the Elbe area is higher than 3m. During the period of the first surge peak (T2, Fig. 11b) the maximum occurs in Sylt-Römo Bight area (above 2.8 m) and along the Elbe and Weser estuaries (about 2.5 m), however over the whole German Bight area the simulated surge is above 1.5 m. In the period of relative calm conditions before the storm (T1), the surge is relatively low (Fig. 11a, less than 30 cm). A decrease of the surge in direction north-western German Bight is simulated during T4 (Fig. 11d). The intensification of the storm surge from open sea towards the coastal area is consistent with the specific atmospheric conditions during Xaver (Fig. 3).

To better understand the impact of the processes of wave-circulation interaction on the surge simulations we will also analyse the horizontal patterns of the maximum differences of the storm surge between the coupled model (FULL run) and the stand-alone GETM (CTRL run). The maximum differences for each grid point are estimated over the four tidal periods (Fig. 12, T1-



T4). The patterns show that the differences between the FULL and CTRL runs during the first surge maximum are more noticeable at the low-lying North-Frisian Wadden Sea. The maximum surge simulated by the fully coupled model exceeds the one of the CTRL run with ca 60 cm along the Sylt-Römo Bight during the T2 period. The enhancement of the surge in the coastal area (see Fig. 11b) is due to the non-linear interactions processes between circulation and waves (the contribution of the wave-current interaction of the increase of the surge is more than 25%) along the German Bight coastal region (Fig.12a). For the T3 period the maximum surge difference (of about 55 cm) is concentrated along the Elbe river area; however over the whole German Bight coast the increase of the surge due to wave-induced processes exceeds 40 cm. During the second Xaver peak, the radiation stress contributes to a rise of the sea level along the whole German Bight coast and in direction to the Elbe-Weser river area. For the first peak (T1) the differences between FULL and CTRL run are more pronounced towards the North Frisian Wadden Sea. The computed maximum surge differences are higher during the period T2 than the ones obtained during the period T3. For T4 (Fig. 12d) the maximum difference of ca 15 cm occurs for the east Frisian coast toward the Elbe area, whereas along the north eastern part the wave-induced processes do not contribute much to the mean sea level and the surge simulation of the FULL runs are similar to the CTRL ones. The horizontal distribution of the patterns of Fig. 12 demonstrates the good consistency with the meteorological situation (Fig. 3). The effects of wave-induced forcing during the storm are also observed in the open North Sea (maximum surge differences are about 30 cm Fig. 12b, c) and are due to the dominant role of the radiation stress - even in the deeper areas the differences between FULL and CTRL surge estimates are more than 20%. Even though the wave heights were much higher in the open sea, the water there is much deeper and thus the differences in sea level between FULL and CTRL runs are relatively small.

### 5.2 3-D versus 2-D barotropic models

Depth average two-dimensional flow models are widely applied in storm surge simulation, and have been assumed to meet the requirement of the operational forecasts and of most scientific studies. However, to study the flow characteristics of the storm surges the use of barotropic models only could be inappropriate, in particular in the large discharge estuaries. The flows in the surface and bottom layers are usually quite different, so that the depth average two-dimensional model cannot sufficiently depict the flow structure. Even more, storm surge models



do not account for the baroclinic processes, like the density-driven changes of the water masses, which is important in the estuarine environments.

The changes of the sea level due to temperature for Nederland coastal areas have been studied by Tsimplis et al. (2006). Dangendorf et al. (2013) showed that laterally forced steric variation and baroclinic processes became important at decadal scales while atmospheric forcing causes the annual variability of the sea level. Recently, Chen et al (2016) studied the role of the of remote baroclinic and local steric effects to the interannual sea level variability and found that the three-dimensional model that consider temperature and salinity can better simulate the North Atlantic Oscillation (NAO) related changes of the water level. In these models more realistic open boundary conditions (than in the barotropic models) are used that allow accounting for the dynamics of heat and salt. In this section, the role of using a fully three-dimensional model that also consider temperature and salinity, when simulating the sea level during extremes will be analysed.

The patterns providing the differences between FULL and 2D runs confirm firstly that those differences are much larger during the storm Xaver (T2, Fig.13b) than for the calm conditions (T1, Fig. 13a). For T2 the maximum difference grows eastward from 2-5 cm at the western boundary of the German Bight to more than 80 cm along the North –Frisian Wadden Sea coast and near the Elbe and Weser estuaries. Those surge differences decrease to 30 cm during the second peak of Xaver. After the storm, the three-dimensional effects contribute to an increase in the sea level in the direction of the Elbe estuary (Fig. 13d). Those effects can reach more than 25% of the sea level increase in comparisons to the 2D model simulations (Fig, 14). For the Elbe area the 2D model underestimates the mean sea level with about 1 m. This could cause significant underestimation of the sea level predictions performed by barotropic models only. For T4 the impact of baroclinicity is localized along the south-eastern coastline (Fig. 13d). The differences between FULL and NORIV runs (Fig.14. blue line) are negligible at station ST3 while for the ST6 they are about 15 cm during storm Xaver in the vicinity of Elbe estuary.

## 6. Discussion and conclusions

With the uncertainties of storm surge predictions under climate change, the quantification of associated hazard is of great interest to the coastal area. The demand to know what changes in the risks and losses can be expected when developing different future projections increases.



Although storm surge forecasting technology has been gradually mature, the accurate real time assessment of the storm surge and inundation area is still defective to satisfy the demands because the real time storm forecasting, as the important driving force of surge, is not perfect in practical use. It always leads to a high degree of uncertainty in storm surge forecasting until the final moment. The peak surge is depended on the accurate landfall position and time. Since the astronomical tide may has a huge tide range in some coastal areas during the storm surge, the uncertainty of forecasting cause a dilemma in hazard relief. The future development of water level predictions will focus on both enlarging the observation data network and further model developments. To reduce uncertainty, increasing the knowledge on the processes like tide-wave-surge interactions, is needed. Improved weather forecast and also further coupling between atmosphere, ocean and wave components will reduce the uncertainties. Increasing the horizontal resolution for the near coastal areas is made possible with availability of more computational resources. In this study we show that wave-dependent approach yields to 25% larger surge at the whole coastal area of the German Bight reaching a contribution of about 40% is some coastal area during extremes. The contribution of the fully 3-D model in comparison with a 2D barotropic one yield to 20% differences in the water level of the coastal areas of the German Bight during Xaver.

Nowadays new observations are available, using the remote sensing of wind speed, waves, sea levels and currents; X-band and HF-radar, ADCP, LIDAR, Ku and Ka band pulse-limited and Delay Doppler radar altimetry, which promise high quality space observations also in the coastal zone. Better sea level data near the landfall and storm variables are demanded by a closer network of tide gauges and buoys and by observations from space. According to the balance of investment and the demand of disaster relief, some more tide gauge stations should be established in empty or sparse areas. The newly available satellite products are expected to improve the forecasting model systems (both in ocean and atmosphere). For the coastal areas the role of wave-induced forcing on coastal morphology is also subject of further study.

We showed here that interaction between waves and three dimensional hydrodynamical models reduces the forecast errors, especially during extreme events. This will enable further use of the high resolution coupled model system for both improving the coastal flooding predictions as well as climate studies.



### **Acknowledgements:**

This work has been supported through the Coastal Observing System for Northern and Arctic Seas (COSYNA) and as part of the Copernicus Marine Environment Monitoring Service (CMEMS) Wave2Nemo project. CMEMS is implemented by Mercator Ocean in the framework of a delegation agreement with the European Union. Luciana Fenoglio is supported by the European Space Agency (ESA) within the Climate Change Initiative (CCI). The authors are thankful to I. Nöhren for assistance with the graphics, and to BSH for providing the observational data.



## References

- Ardhuin, F., Rasche, N., Belibassakis, K.: Explicit wave-averaged primitive equations using a generalized Lagrangian mean, *Ocean Modell.*, 20 (1), 35–60, 2008.
- Ardhuin, F, Rogers, E, Babanin, AV, Filipot, J-F, Magne, R, Roland, A, van der Westhuysen, A, Queffelec, P, Lefevre, J-M, Aouf, L, Collard, F (2010) Semiempirical dissipation source functions for ocean waves Part I: definition, calibration, and validation. *J. Phys. Oceanogr.* 40, 1917–1941
- Babanin, A V, (2006) On a wave-induced turbulence and a wave-mixed upper ocean layer. *Geophys Res Lett*, 33 (20), 6, doi:10.1029/2006GL027308
- Babanin, A. V., Chalikov, D., Young, I. R., and Savelyev, I.: Numerical and laboratory investigation of breaking of steep two- dimensional waves in deep water, *J. Fluid Mech.*, 644, 433–463, 2010.
- Barbariol, F, Benetazzo, A, Carniel, S and Sclavo, M, (2013) Improving the assessment of wave energy resources by means of coupled wave-ocean numerical modeling. *Renew. Energ.* 60, , 462–471.
- Benetazzo, A, Carniel, S, Sclavo M. and Bergamasco, A., Wave-current interaction: effect on the wave field in a semi-enclosed basin. *Ocean Model.* 70, 152–165
- Bennis, A., and Ardhuin, F.: Comments on the depth-dependent current and wave interaction equations: a revision, *J. Phys. Oceanogr.*, 41, 2008–2012, 2011.
- Bidlot, J.-R., Janssen P., Abdalla S., and Hersbach H.: A revised formulation of ocean wave dissipation and its model impact, ECMWF Tech. Memo. 509 , Eur. Cent. for Medium-Range Weather Forecasting, Reading, UK, 2007.
- Bolaños, R., Osuna, P., Wolf, J., Monabiu, J., Sanchez-Arcilla, A.: Development of the POLCOMS–WAM current–wave model, *Ocean Model.*, 36, 102–115, 2011.
- Bolaños, R.; Brown, J.M.; Souza, A.J.: Wave-current interactions in a tide dominated estuary. *Continental Shelf Research*, 87. 109-123. 10.1016/j.csr.2014.05.009, 2014.



- Brown J.M., Bolaños R., and Wolf J.: Impact assessment of advanced coupling features in a tide-surge-wave model, POLCOMS-WAM, in a shallow water application, *J Mar Syst* 87(1), 13–24, 2011.
- 5 Brown J.M., Bolaños R., and Wolf J.: The depth-varying response of coastal circulation and water levels to 2D radiation stress when applied in a coupled wave-tide-surge modelling system during an extreme storm, *Coast Eng.*, 82:102–113, 2013.
- Brown, JM, Wolf, J, (2009) Coupled wave and surge modelling for the eastern Irish Sea and implications for model wind-stress. *Cont. Shelf Res.* 29 (10), 1329–1342
- 10 Burchard, H. and Bolding K.: GETM - a General Estuarine Transport Model, No EUR 20253 EN, printed in Italy, European Commission, 2002.
- Chen, X., Dangendorf S., Narayan N., O'Driscoll K., Tsimplis M., Su J., Mayer B. and Pohlmann T. (2014) On sea level change in the North Sea influenced by the North Atlantic Oscillation: Local and remote steric effects. *Estuarine Coastal and Shelf Science*, 151, 186-195. (doi:10.1016/j.ecss.2014.10.009).
- 15 Dangendorf S., A Arns, JG Pinto, P Ludwig, J Jensen, The exceptional influence of storm 'Xaver' on design water levels in the German Bight, *Environmental Research Letters*, 2016
- Donelan, M A, J Hamilton, and W H Hui, (1985) Directional spectra of wind generated waves. *Phil Trans R Soc Lond A*, 315, 509{562, doi:10.1098/rsta. 1985.0054
- 20 Deuschländer T, Friedrich K, Haeseler S and Lefebvre C. (2013) Severe storm XAVER across northern Europe from 5 to 7 December 2013, December, 2013 DWD report, <https://www.dwd.de/EN/ourservices/specialevents/storms>
- Fan, Y, I Ginis, and T Hara (2009) The effect of wind-wave-current interaction on air-sea momentum fluxes and ocean response in tropical cyclones, *J Phys Oceanogr*, 39 (4), 1019– 1034, doi:10.1175/2008JPO4066.1
- 25 Fenoglio-Marc, L., R. Scharroo, A. Annunziato, L. Mendoza, M. Becker, and J. Lillibridge, Cyclone Xaver seen by geodetic observations, *Geophys. Res. Lett.*, 42, 9925–9932, doi:10.1002/2015GL065989, 2015.
- Flather, RA, (2001) Storm surges. In: Steele, J., Thorpe, S., Turekian, K. (Eds.), *Encyclopedia of Ocean Sciences*. Academic, San Diego, California, pp. 2882–2892



- Grashorn, S., Lettmann, K.A., Wolff, J.-O., Badewien, T.H., Stanev, E.V.: East Frisian Wadden  
Wea hydrodynamics and wave effects in an unstructured-grid model, *Ocean Dynamics* 65 (3),  
419–434, 2015.
- Günther, H., S. Hasselmann, P.A.E.M. Janssen, The WAM Model Cycle 4.0. User Manual.  
5 Technical Report No. 4, Deutsches Klimarechenzentrum, Hamburg, Germany. 102 pages, 1992.
- Horsburgh, K.J. and Wilson, C. 2007 Tide-surge interaction and its role in the  
distribution of surge residuals in the North Sea. *Journal of Geophysical Research*, 112, C08003,  
doi:10.1029/2006JC004033
- Huang, C J, F Qiao, Z Song, and T Ezer, Improving simulations of the upper ocean by inclusion  
10 of surface waves in the Mellor-Yamada turbulence scheme, *J Geophys Res*, 116 (C1),  
doi:10.1029/2010JC006320, 2011.
- Hersbach, H. and Janssen P.: Improvements of the short fetch behaviour in the WAM model, *J.*  
*Atmos. Oceanic Techn.*, 16, 884-892, 1999
- Janssen, P, The interaction of ocean waves and wind, 300 pp., Cambridge University  
15 Press, Cambridge, UK, 2004.
- Jensen, J. and Mueller-Navarra, S.H. Storm Surges on the German Coast, *Die Küste*, ICCE,  
2008.
- Jones, J. E. & Davies, A. M., Storm surge computations in estuarine and near-coastal regions: the  
Mersey estuary and Irish Sea area, *Ocean Dynamics*, 59, 6; 1061-1076, 2009.
- 20 Katsafados P, Papadopoulos A, Korres G, and Varlas G, A fully coupled atmosphere–ocean  
wave modeling system for the Mediterranean Sea: interactions and sensitivity to the resolved  
scales and mechanisms, *Geosci. Model Dev.*, 9, 161–173www.geosci-model-  
dev.net/9/161/2016/doi:10.5194/gmd-9-161, 2016.
- Komen, G.J., Cavaleri L, Donelan M, Hasselmann K, Hasselmann S. and P. Janssen: Dynamics  
25 and modelling of ocean waves, Cambridge University Press, Cambridge, UK, 560 pages, 1994.
- Kumar, N.,Voulgaris, G., Warner, J.C., and Olabarrieta,M.: Implementation of the vortex force  
formalism in the coupled ocean–atmosphere–wave–sediment transport (COAWST) modelling  
system for inner shelf and surf zone applications, *OceanModel.*, 47, 65–95, 2012.



- Lane, E.M., Restrepo, J.M., and McWilliams, J.C.: Wave–current interaction: a comparison of radiation-stress and vortex-force representations, *J. Phys. Oceanogr.* 37 (5), 1122–1141, 2007.
- Lettmann K., Wolff J-O, and Badewien T.: Modeling the impact of wind and waves on suspended particulate matter fluxes in the East Frisian Wadden Sea (southern North Sea), *Ocean Dyn.*, 59(2), 239–262, 2009.
- 5 Longuet-Higgins M.S., and Stewart R.W.: Radiation stresses in water waves: a physical discussion with applications, *Deep-Sea Res.*, 11, 529–562, 1964.
- McWilliams, J., Restrepo, J., and Lane, E.: An asymptotic theory for the interaction of waves and currents in coastal waters, *J. Fluid Mech.*, 511, 135–178, 2004.
- 10 Mellor G.: The three-dimensional current and surface wave equations, *J Phys. Oceanogr.* 33(9), 1978–1989, 2003.
- Mellor G.: Some consequences of the three-dimensional current and surface equations. *J. Phys. Oceanogr.* 35(11), 2291–2298, 2005.
- Mellor G.: The depth-dependent current and wave interaction equations: a revision, *J. Phys.*  
15 *Oceanogr.* 38(11), 2587–2596, 2008.
- Mellor G.: Wave radiation stress. *Ocean Dyn.* 61(5), 563–568, 2011.
- Mellor G.: Waves, circulation and vertical dependence. *Ocean Dyn* 63(4), 447–457, 2013.
- Michaud, H., Marsaleix, P., Leredde, Y., Estournel, C., Bourrin, F., Lyard, F., Mayet, C., and Arduin, F., 2012: Three-dimensional modelling of wave-induced current from surf zone to the  
20 inner shelf, *Ocean Sci.*, 8, 657–681, 2012.
- Osuna, P., Souza, A.J. and Wolf, J., Effects of the deep-water wave breaking dissipation on the wind-wave modelling in the Irish Sea. *Journal of Marine Systems*, 67 (1-2). 59-72. 10.1016/j.jmarsys.2006.09.003, 2007
- Pawlowicz, R., Beardsley B., and Lent S.: Classical tidal harmonic analysis including error estimates in MATLAB using T-TIDE, *Comput. Geosci.*, 28 8, 929-937, doi10.1016/S0098-3004(02), 2002
- 25 Pleskachevsky, A., Dobrynin, M.; Babanin, A. V.; Günther, H., and Stanev, E.: Turbulent mixing due to surface waves indicated by remote sensing of suspended particulate matter and its



- implementation into coupled modeling of waves, turbulence and circulation. *Journal of Phys. Oceanogr.* 41 (4), S. 708-724. doi: 10.1175/2010JPO4328.1, 2011
- Pullen, T., Allsop, N.W.H., Bruce, T., Kortenhaus, A., Schüttrumpf, H. and van der Meer, J.W., Eurotop - Wave Overtopping of Sea Defences and Related Structures: Assessment Manual. [www.overtopping-manual.com](http://www.overtopping-manual.com), 2007
- 5 Qiao, F, Y, Yuan, Y. Yang, Q. Zheng, C. Xia, and J. Ma, Wave-induced mixing in the upper ocean: Distribution and application to a global ocean circulation model. *Geophys Res Lett*, 31 (11), 4, doi:10.1029/2004GL019824, 2004.
- Röhrs, J., Christensen, K. H., Hole, L. R., Broström, G., Drivdal, M. & Sundby, S.: Observation-based evaluation of surface wave effects on currents and trajectory forecasts. *Ocean Dynam.*, 62, 10 1519-1533, 2012.
- Röhrs, J., Christensen, K. H.; B., V. F.; Sundby, S.; Saetra, O., Broström, G.: Wave- induced transport and vertical mixing of pelagic eggs and larvae. *Limnol. Oceanogr.*, 59(4), 1213-1227, 2014.
- 15 Roland A., and Ardhuin F, On the developments of spectral wave models: numerics and parameterizations for the coastal ocean. *Ocean Dyn* 64, 6, 833–846, 2014.
- Rossiter, J. R. (1958), Storm surges in the North Sea, 11 to 30 December 1954, *Phil. Trans. R. Soc. Lond.*, 251 991, 139-160, doi:10.1098/rsta.1958.0012. ,
- Scharroo, R., Leuliette, E.W., Lillibridge, J.L., Byrne, D., Naeije, M.C., Mitchum, G.T.: RADS: consistent multi-mission products. In: *Proc. of the Symposium on 20 Years of Progress in Radar Altimetry*, ESA SP-710. ESA Spec. Publ., 2013
- 20 Stanev, E. V., Schulz-Stellenfleth, J., Staneva, J., Grayek, S., Seemann, J., and Petersen, W: Coastal observing and forecasting system for the German Bight—estimates of hydrophysical states, *Ocean Sci.*, 7, 569-583, 2011.
- 25 Staneva, J., E. Stanev, J.-O. Wolff; T.H. Badewien; R. Reuter; B. Flemming; A. Bartholomae and K. Bolding: Hydrodynamics and sediment dynamics in the German Bight. A focus on observations and numerical modeling in the East Frisian Wadden Sea, *Cont. Shelf Res.*, 29, pp. 302-319, 2009.



- Staneva J, Wahle K Günther H and Stanev E: Coupling of wave and circulation models in coastal-ocean predicting systems: A case study for the German Bight, MS No.: OS-2015-86, Ocean Sci., 12, 797-806, doi:10.5194/os-12-797-2016, 2016
- 5 Styles, R., and Glenn, S.: Modeling stratified wave and current bottom boundary layers on the continental shelf, J. Geophys. Res. 105, C10, 24119–24124, 2000.
- Uchiyama, Y., McWilliams, J., and Shchepetkin, A.: Wave-current interaction in an oceanic circulation model with a vortex-force formalism: application to the surf zone, Ocean Modell. 34, 16–35, 2010.
- 10 Valecke S., Craig T., Coquart L.: OASIS3-MCT User Guide, OASIS3-MCT 2.0. Technical Report, TR/CMGC/13/17, CERFACS/CNRS SUC URA No 1875, Toulouse, France (2013).
- Weber, J.E., Broström, G, and Christensen, K.H., “Radiation stress and the depth-dependent drift in surface waves with dissipation”, Int. J. Offshore and Polar Eng. 18, (1), 8-13 (2008). Warner, J.C., Sherwood, C.R., Arango, H.G., and Signell, R.P.: Performance of four turbulence closure models implemented using a generic length scale method, Ocean Modell. 8 (1–2), 81–113, 2005.
- 15 Wolf, J., Brown, J.M., Bolaños, R., and Hedges, T.: Waves in coastal and estuarine waters. In: Eric, Wolanski, Donald, McLusky (Eds.), Treatise on Estuarine and Coastal Science, Vol.2. Elsevier, 171–212, 2011.
- Wolf, J., and Prandle, D.: Some observations of wave-current interaction, Coast. Eng. 37, 471–485, 1999.
- 20



Experiment	3-D GETM	WAM	Barotropic	Rivers run-off
CTRL	yes	-	-	yes
FULL	yes	Two-way	-	yes
FORCED	yes	One-way	-	yes
2D	-	-	yes	no
NORIV	yes	yes	-	no

**Table 1.** Model experiments.

5

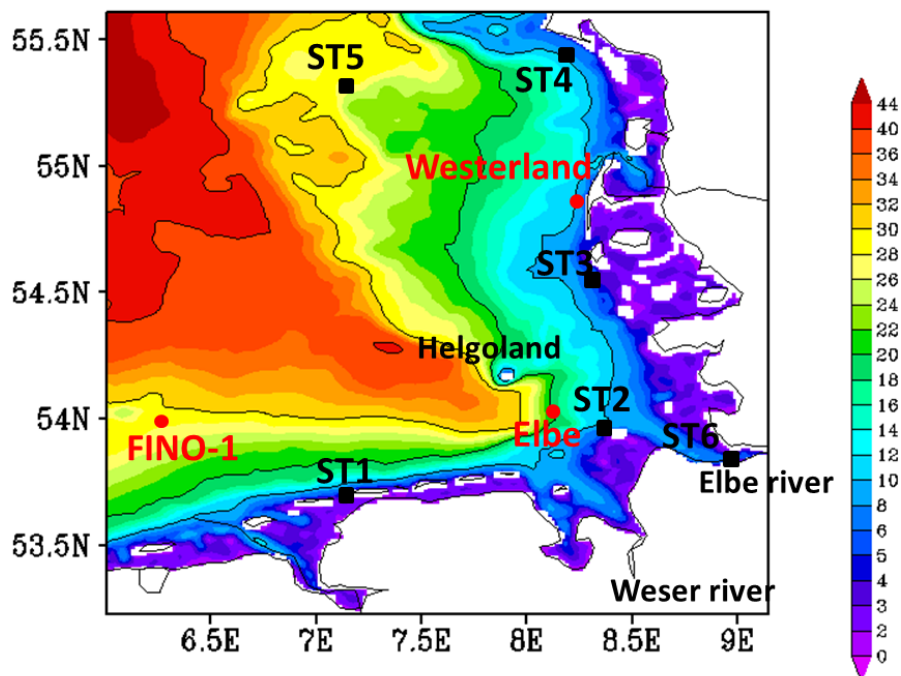
	CTRL	FULL	FORCED	2D
<b>RMSE</b>	0.26	0.16	0.15	0.39
<b>Bias</b>	-0.17	-0.09	-0.10	-0.28
<b>Correlation</b>	0.84	0.92	0.93	0.76

**Table 2.** Surge (m): Root-Mean Square Errors (RMSE), bias (model-observations) and correlation between storm surge component from four model runs (CTRL, FULL, FORCED and 2D) and from tide gauge records of the British Oceanographic Data Centre (BODC) over the German Bight area.

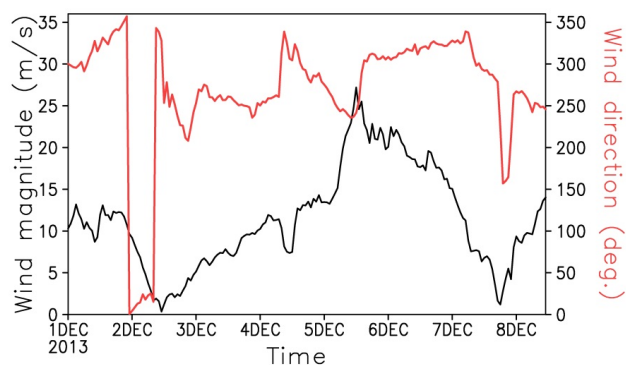
10



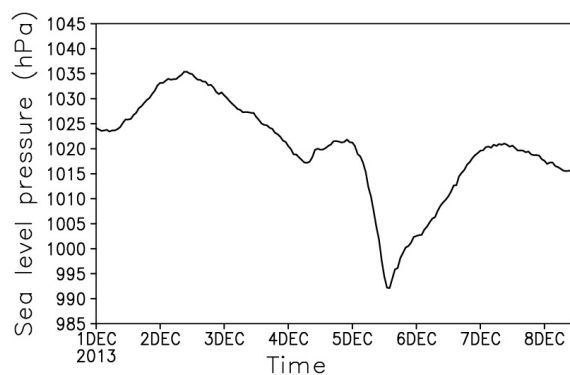
## Figures



- 5 **Figure 1.** German Bight bathymetry (contour lines correspond to isobaths 10 m, 20 m, 30 m and 40 m). The geographical location of stations analysed later are shown as well. The wave data stations are plotted in red circles; the stations in which we analyse the sea level variability (ST1-6) are plotted in black squares.



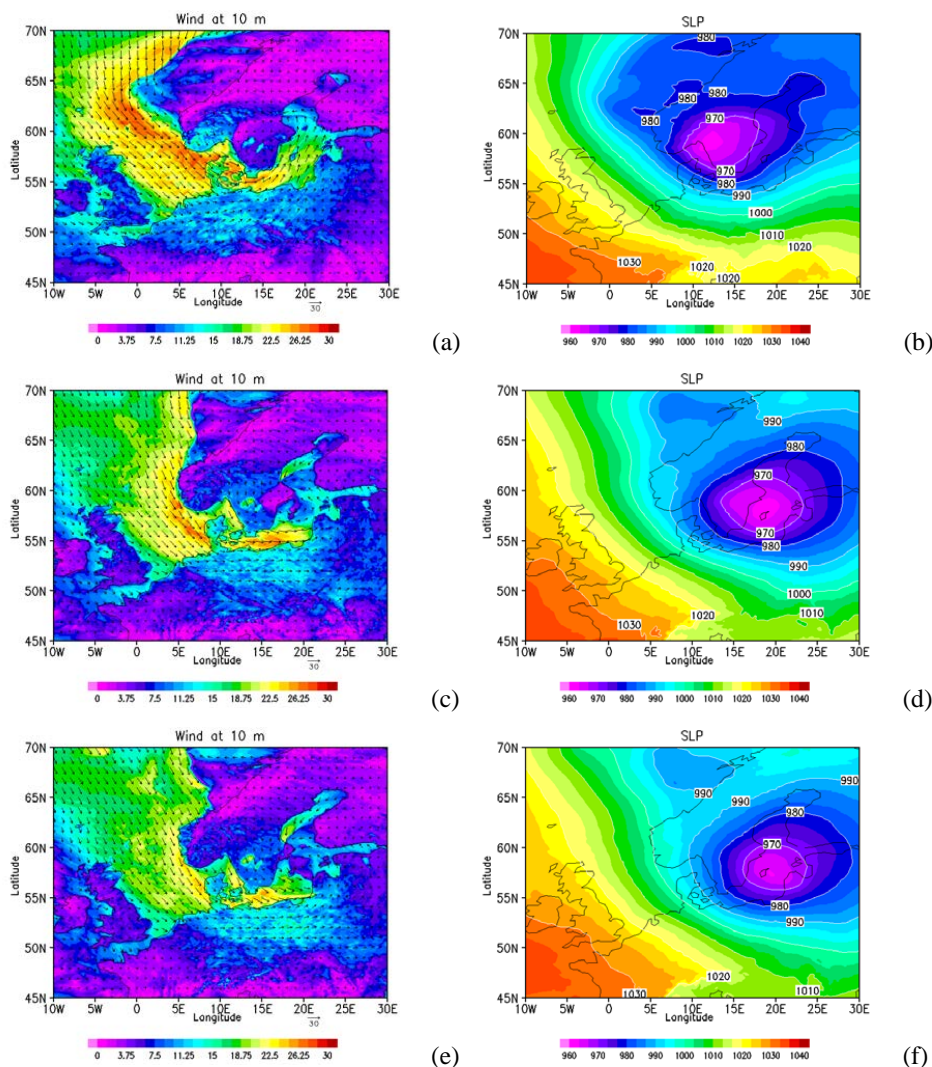
(a)



(b)

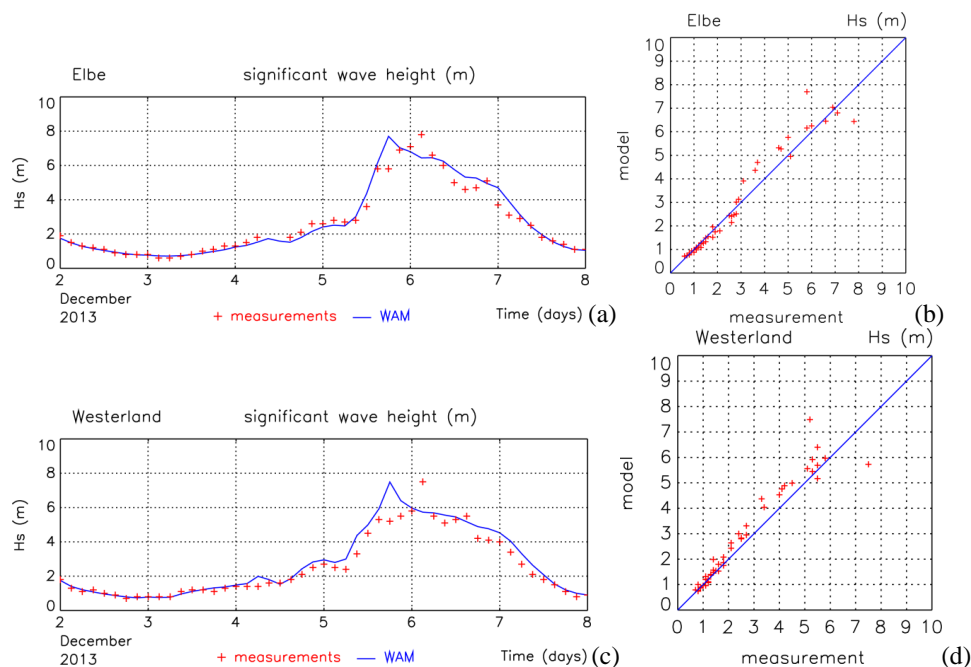
**Figure 2.** Meteorological situation at Elbe Station (see Figure 1 for its location) during Storm Xaver from the DWD data.

- 5 (a) 10 m wind magnitude (black line) and wind direction (red line);  
(b) atmospheric pressure.



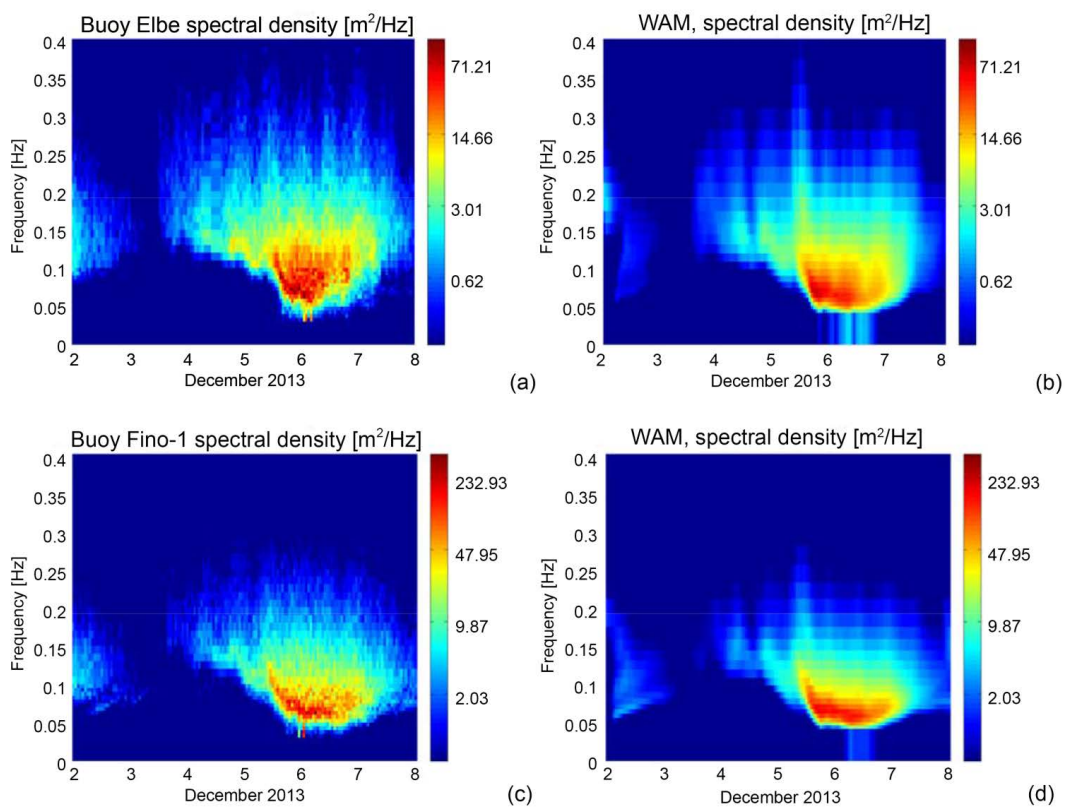
5 **Figure 3.** Meteorological situation during Storm Xaver:

- (a) DWD 10 m wind magnitude [m/s] (in colour) and wind direction (arrows) on 05.12.2013 at 18:00;
- (b) Sea level pressure [hPa] on 05.12.2013 at 18:00;
- (c) same as (a) but on 06.12.2013 at 03:00;
- (d) same as (b) but on 06.12.2013 at 03:00;
- 10 (e) same as (a) but on 06.12.2013 at 07:00;
- (f) same as (b) but at 06.12.2013 at 07:00.



5

**Figure 4.** Time series (left) and scatter plots (right) of observed (red) and simulated (blue) significant wave height at the Elbe (top) and Westerland (bottom) buoy stations. See Fig. 1 for locations.



5 **Figure 5.** Comparison of measured (left) and computed (right) values of the spectral energy density at the buoy Elbe (top) and buoy 'FINO1 (bottom) (see Fig. 1 for locations).

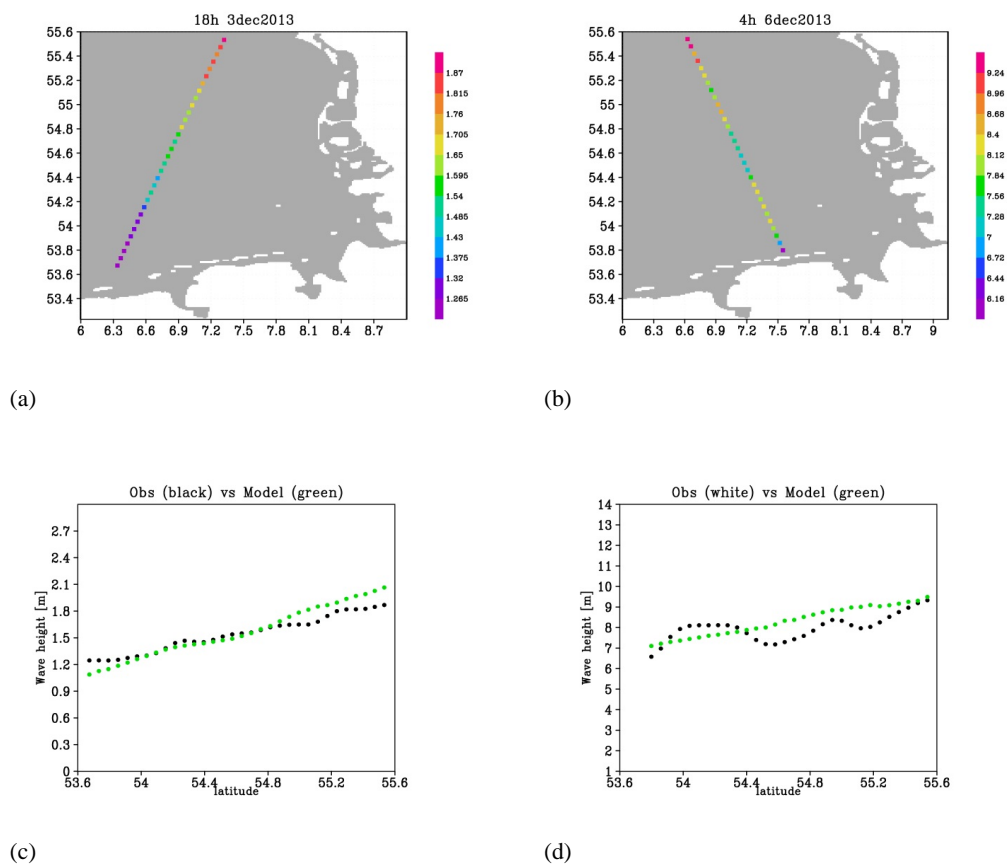
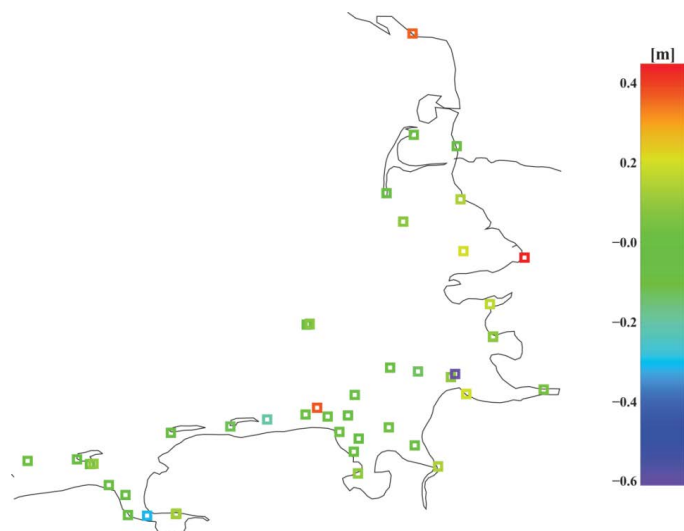
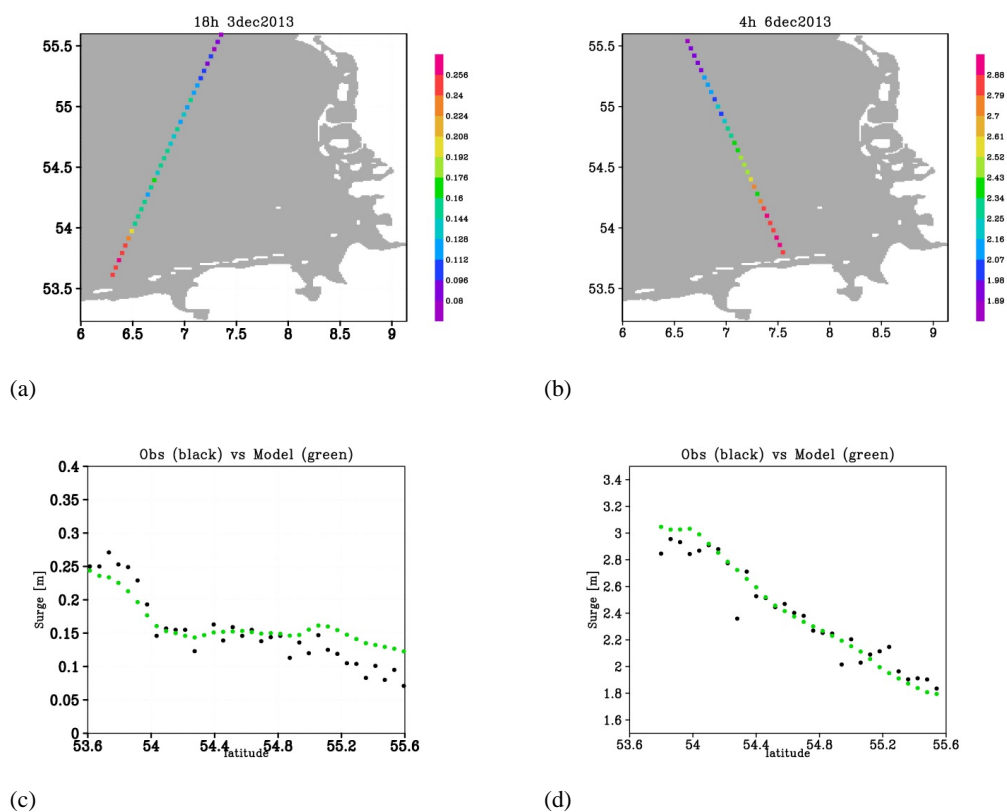


**Figure 6.** Along-track observed and modelled significant wave heights (m).  
 (a) SARAL/AltiKa ground-track for over-flight in calm conditions at 03.12.2013 on 18:00 UTC, in colours are  
 observed altimetric significant wave height (m);  
 (b) same as (a) but during storm Xavier on 06.12.2013 at 04:00 UTC;  
 (c) observed (black) and modelled from WAM model (green) significant wave height (m) on 02.12.2013 on 18:00;  
 (d) same as (c) but during storm Xavier on 06.12.2016 at 04:00 UTC.



5

**Figure 7.** Bias (m) between the model simulations and observations for the mean sea level averaged over the whole period of integration.

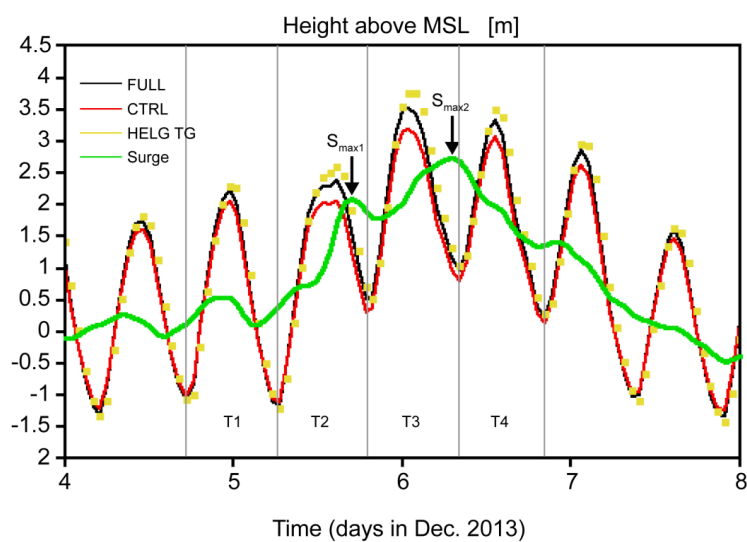


5

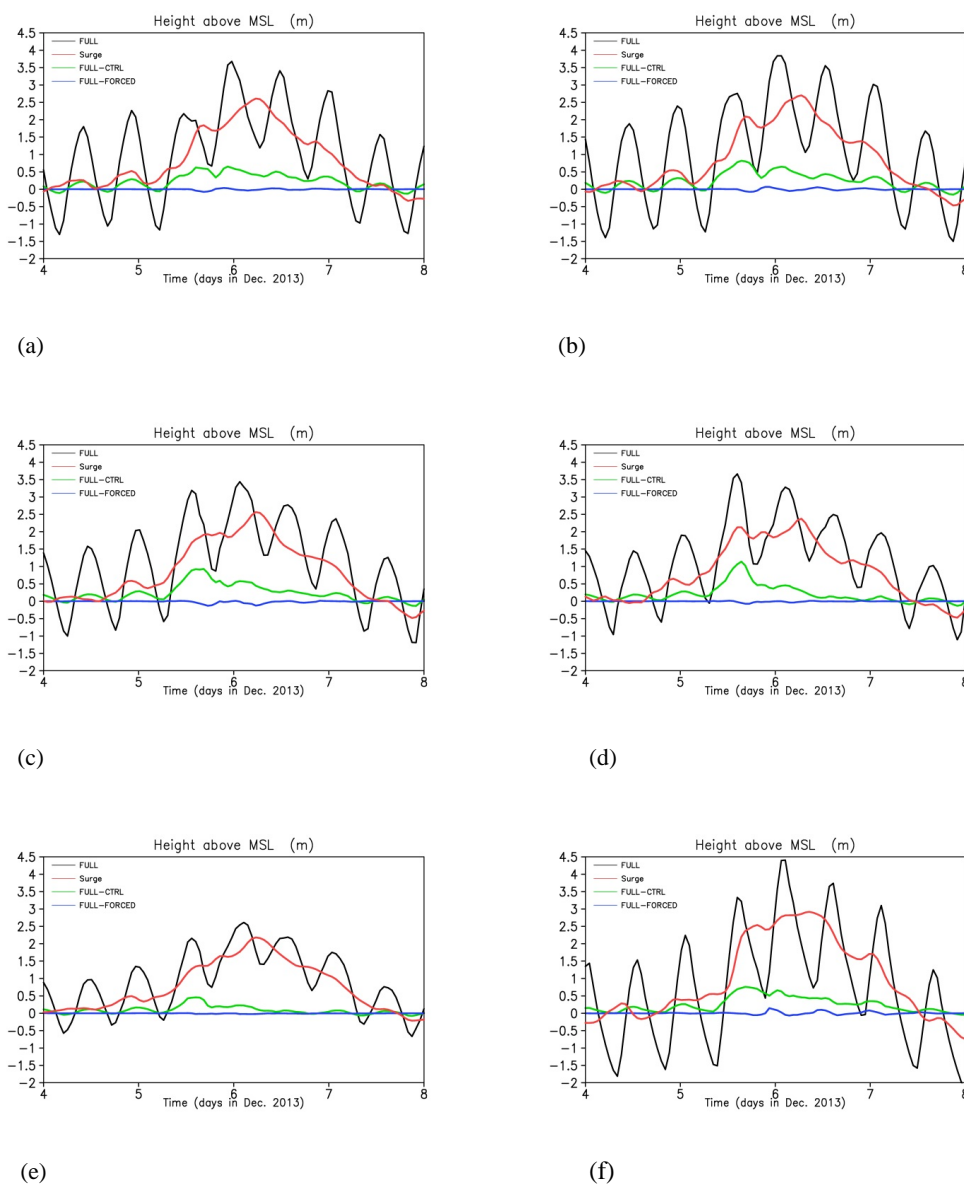
**Figure 8.**

- (a) Surge at the time of the SARAL overflight in calm conditions on 03. December 2013 at 18:00;  
 (b) same as (a) but during storm Xaver on 06.12 2013 at 04:00 UTC;  
 10 (c) profiles of SARAL/AltiKa overflight of surge height derived from altimeter observations (black circles ) and  
 from GETM model (green circles) on 03. December 2013 at 18:00;  
 (d) profiles of SARAL/AltiKa overflight of surge height derived from altimeter observations (green circles ) and  
 from GETM model (yellow circles) on 06. December 2013 at 04:00.

15



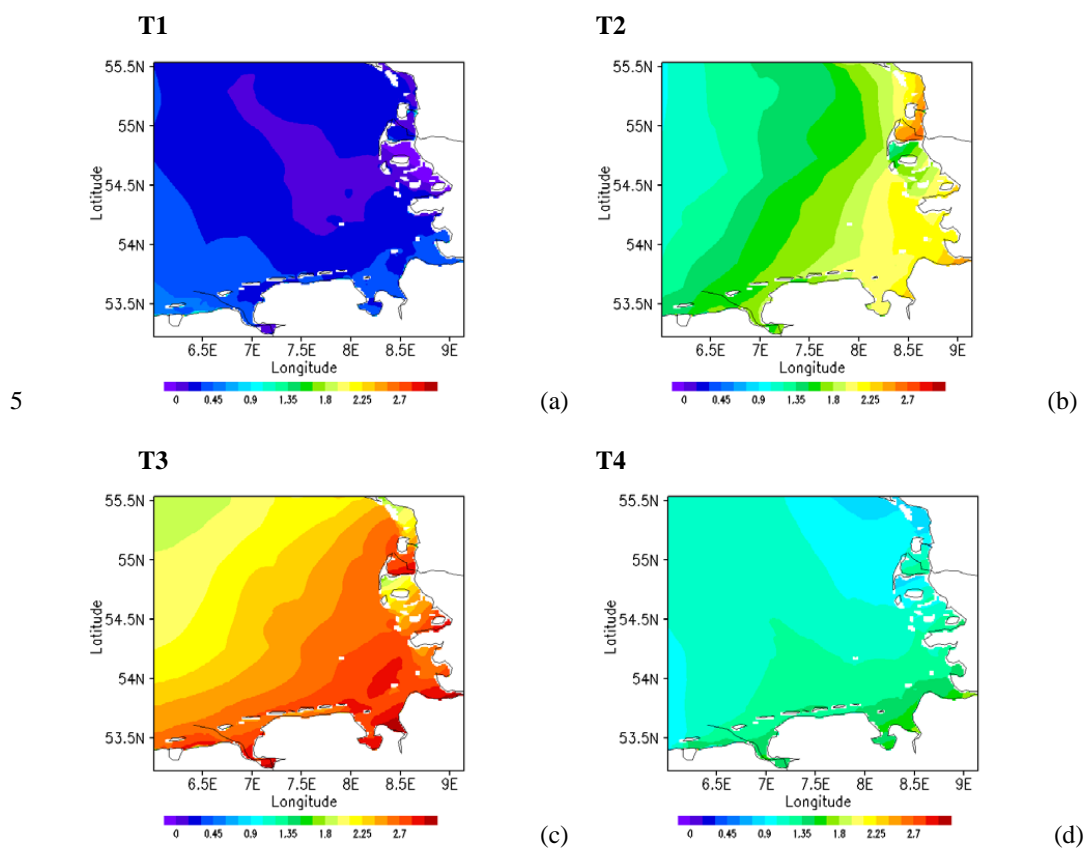
5 **Figure 9.** Time series of the Mean Sea Level (MSL) in [m] at Helgoland station (see Fig. 1 for its location). Yellow dots: line: tide gauge observations, black line: coupled wave-circulation model (WAM-GETM), red line only circulation model (GETM), green line – storm surge.



5

10

**Figure10.** Time series of the Mean Sea Level (MSL-black line); storm surge (red line): differences between the storm surge from FULL and CTRL runs (FULL-CTRL, green line) differences between the FULL and FORCED runs (FULL-FORCED, blue line) at six stations ST1-ST6 (see Fig. 1 for locations).



10 **Figure 11.** Maximum surge in (m) over the four different tidal periods (T1-T4) as shown on Fig. 9.

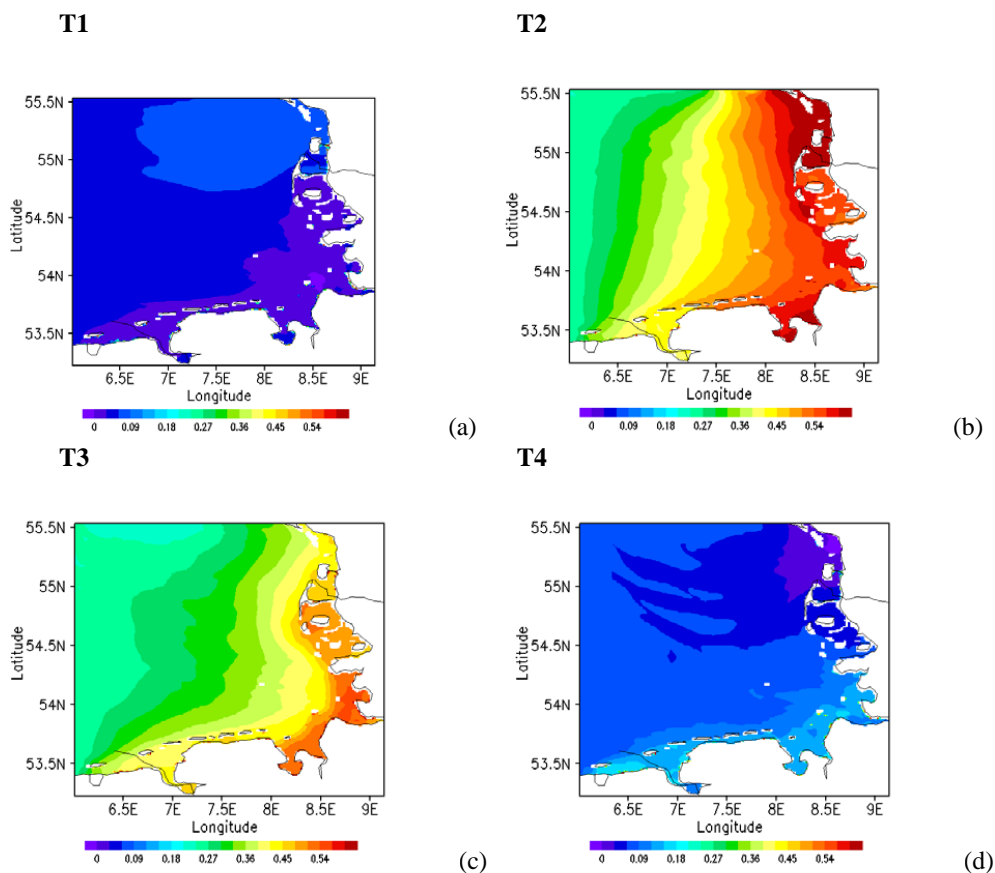
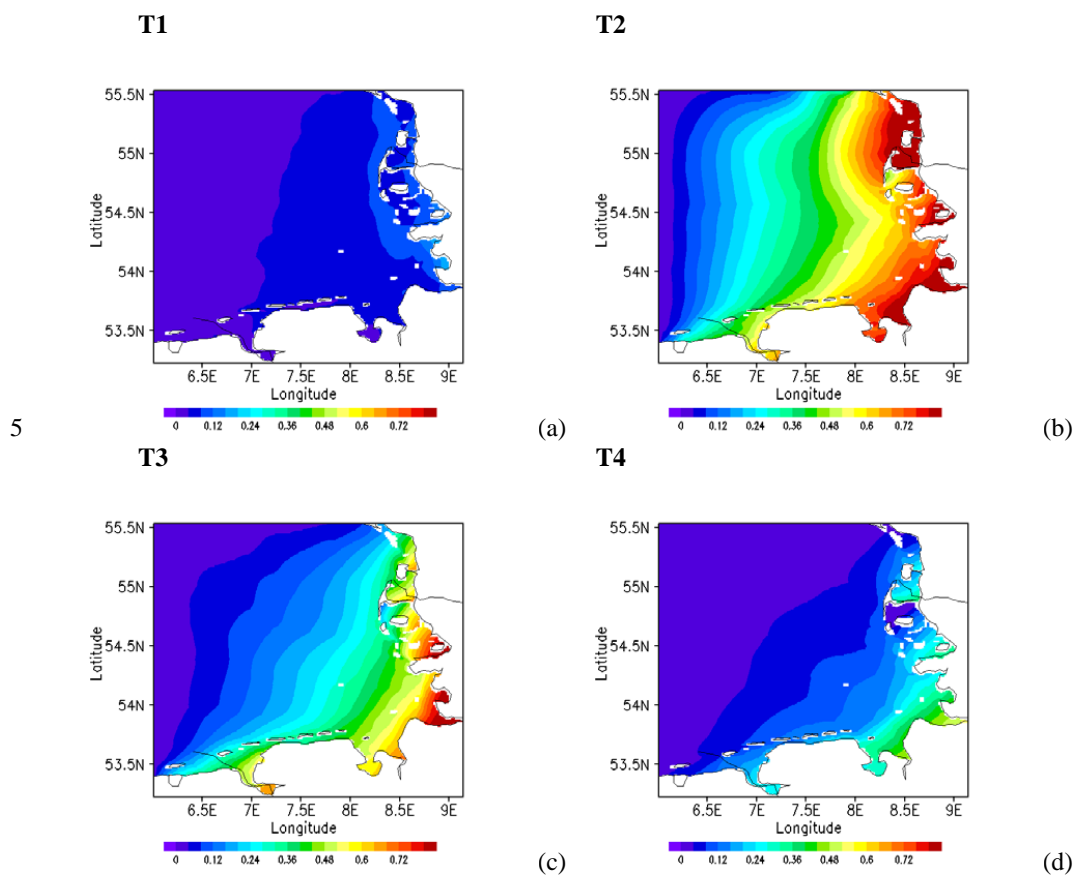
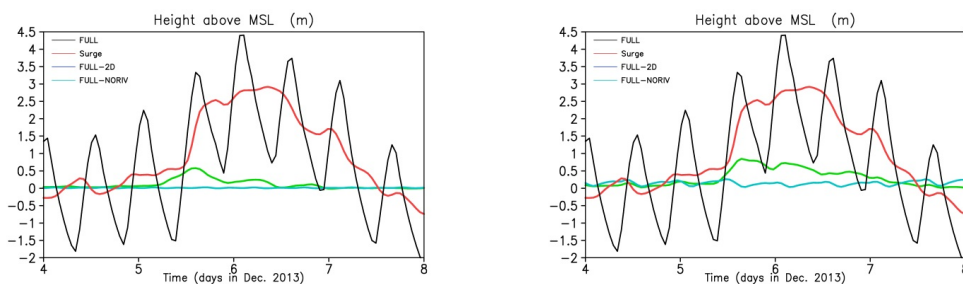


**Figure 12.** Maximum surge differences between FULL and CTRL runs in (m) for T1-T4 tidal periods as shown on Fig. 9.

10



10 **Figure 13.** Maximum surge differences between FULL and 2D runs (in m) for T1-T4 tidal periods as shown on Fig. 9.



(a)

(b)

5

**Figure 14.** The role of the baroclinicity for the sea level variability in ST3 and ST6 stations; for the FULL run (black line); storm surge (red line); differences between the storm surge from FULL and 2D runs (FULL-2D, green line); differences between the storm surge FULL and NORIV runs (FULL-NORIV, blue line).

10